D14

1984

NASA/ASEE SUMMER FACULTY RESEARCH FELLOWSHIP PROGRAM

MARSHALL SPACE FLIGHT CENTER
THE UNIVERSITY OF ALABAMA

THE STRENGTH AND CHARACTERISTICS OF VPPA WELDED 2219-T87 ALUMINUM ALLOY

Prepared by:	Wartan A. Jemian, Ph.D.
Academic Rank:	Professor
University and Department:	Auburn University Mechanical Engineering and Materials Engineering
NASA/MSFC:	
Laboratory:	Materials and Processes
Division:	Process Engineering
Branch:	Metals Processes
NASA Counterpart:	W. A. Wilson
Date:	August 24, 1984
Contract No.:	NASA-NGT-01-002-099 (The University of Alabama)

ACKNOWLEDGEMENTS

The author thanks Mr. W. A. Wilson for providing this opportunity and for help in many ways. His generous encouragement and support are deeply appreciated. This project has been one of those "hoped for" research situations where the observations and experimental results lead directly to a definite conclusion. In this instance, the size of the interdendritic particles accounted for a variation in weld strength.

Mr. Carl Wood was most helpful in providing assistance in many useful ways. His friendship will always be remembered. Vanita Brown made the word processor available and useful, sharing the use of her office so that this report could be finished on time. Messrs. E. Bayless, Bobby Rowe, Dr. A. C. Nunes and Miss L. Johnston were most helpful in providing information and in discussions. J. Sexton and Jeff Norris welded the panels, cut and prepared the test samples, willingly putting up with a number of special requests. W. DeWeese prepared and photographed the sections for metallurgical analysis and G. De Ramus performed the mechanical testing. Mr. Poorman, who is recently retired, and Dr. C. Lovoy also provided helpful insights and Dr. J. W. Montano assisted in analyses and in locating records of past, related work. Finally, J. Coston and D. Nicholas must be thanked for the hours spent searching, with the SEM, for "the largest" particles on fracture surfaces.

THE STRENGTH AND CHARACTERISTICS OF VPPA WELDED 2219-T87 ALUMINUM ALLOY

BY

Wartan A. Jemian, Ph. D.
Professor, Mechanical Engineering and Materials Engineering
Auburn University
Auburn, Alabama

24 August 1984

ABSTRACT

The purpose of this research is to study the variable polarity plasma arc (VPPA) welding process and to identify those factors that control the structure and properties of VPPA welded aluminum alloy 2219-T87. The importance of joint preparation, alignment of parts and welding process variables are already established. Internal weld defects have been eliminated. However, a variation of properties was found to be due to the size variation of interdendritic particles in the fusion zone. These particles contribute to the void formation process, which controls the ultimate tensile strength of the welded alloy. A variation of 150 microns in particle size correlated with a 10 ksi variation of ultimate tensile strength. It was found that all fracture surfaces were of the dimple rupture type, with fracture initiating within the fusion zone.

It was also found that weld strength is improved if welding is done in alignment with the plate rolling direction. The application of water cooled blocks along the weld track produced a small increase in weld strength and toughness. The results of this research are used to assess the relative importance of a number of materials variables.

Introduction

Alloy 2219 was introduced in 1954 (1) to meet the need for a high strength, heat treatable aluminum alloy with retention of structural integrity up to 600 ^{o}F. It withstands higher service temperatures than any other aluminum alloy and retains excellent mechanical characteristics to -423 ^{o}F (20 ^{o}K) in both the welded and unwelded conditions (2). The static mechanical properties of alloy 2219 over this range of temperatures are shown in Figure 1. Nominal room temperature weld test values are also shown. It has a high weldability with 2319 filler metal (7,12). Nominal compositions of these alloys are listed in table 1. It is the principal structural alloy of the space shuttle external tank.

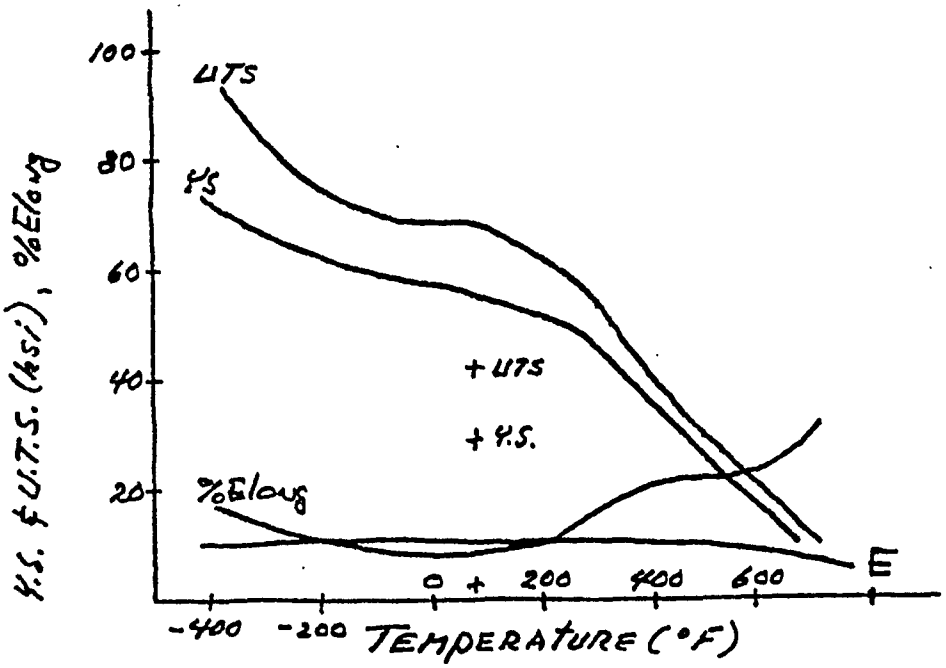

Figure 1. The variation of ultimate tensile strength (UTS), yield strength (YS), percent elongation (%Elong) and Youngs modulus (E) with temperature for alloy 2219-T87 and typical room temperature values for weld test samples (2319 filler wire) (2).

Variable polarity plasma arc (VPPA) welding is a modification of arc welding with special advantages for aluminum alloys. The process features alternating polarity with adjustable arc current, voltage and time in each portion of the cycle. The primary advantage is in the cleaning action of the reverse polarity portion of the cycle (4 msec duration) which removes the oxide layer by bombardment with heavy argon ions, which are a major component of the plasma. In the forward polarity cycle (19 msec) the alloy is heated by impingement of hot electrons, which are another component of the plasma (12). Other advantages, which make VPPA welding useful for many alloy systems, are plasma constraint, which reduces sensitivity to working distance between torch and weld metal and the "keyhole" mode of welding. By controlling beam current and gas flow rate, plasma pressure can be increased to form a stable keyhole which moves with the weld. This keyhole is total penetration through the metal during welding and is filled as the keyhole moves on. Electron beam and laser welding are also keyhole processes. The liquid layer in the keyhole is so thin that gasses released during freezing are swept away rather than being entrapped as porosity in the final joint.

The VPPA process offers many advantages and is now replacing the tungsten inert gas (TIG) welding process that was used initially. To date, in over 24,000 inches of VPPA welds on the space shuttle external tank there has been no internal defect requiring manual preparation and welding (7). Repairing this type of defect represents a major cost in TIG welding.

Process conversion is conducted with great care to ensure that gain in production efficiency is not at the price of weld quality. A rigorous program of TIG/VPPA weld comparisons and study of sensitivity to VPPA process variables is underway. The importance of joint preparation, part alignment and welding process variables are well established and internal welding defects appear to have been totally eliminated. There is, however, a need to identify and explain a residual variation of properties. Possible causes that were considered for investigation include the following factors:

a. geometry
b. chemistry
c. metallurgical structure
d. welding control

Factors within each category were identified and examined

in relation to probable importance and a program of analysis and experimental evaluation was initiated. A portion of this investigation involved review of weld test results from ongoing tests at Marshall Space Flight Center (MSFC) and Michoud Assembly Facility/Martin Marietta Company (MAF/MMC). Other experimental procedures were planned and performed specifically for this study.

The purpose of this research is to study the VPPA process as it applies to the structural weldability of aluminum alloy 2219-T87. Structural weldability is a measure of the level of strength that can be achieved through welding in a system (material and process). Weldability, by the usual meaning, is the capacity to be welded without cracking.

Two specific goals are to identify, on the basis of welding physical metallurgy, the highest strength attainable in welding this alloy system, and to evaluate or estimate the consequences on weld properties associated with the variation of processing controls.

Table 1
Nominal Compositions of Alloys (2,6)

Chemical Element	Alloy 2219	Alloy 2319	Alloy M-934
Silicon	0.20 max	0.20 max	2.05
Iron	0.30 max	0.30 max	0.15
Copper	6.3	6.3	6.7
Manganese	0.3	0.3	0.73
Magnesium	0.02 max	0.02 max	1.51
Zinc	0.10 max	0.10 max	-
Titanium	0.06	0.15	0.06
Vanadium	0.10	0.10	0.01
Zirconium	0.18	0.18	0.17
Beryllium	none	0.0008 max	-
Others, each	0.05 max	0.05 max	
total	0.15 max	0.15 max	
Aluminum	remainder	remainder	remainder

Metallurgical Characteristics

1. Composition.

Copper is the principal alloying element in 2219 and other 2000 series aluminum alloys. The binary phase diagram (Figure 2) shows an eutectic transformation at 548 ^{o}C with solid solution, eutectic and intermetallic compound ($CuAl_2$) compositions of 5.7, 33.2 and 52.5% Cu (by weight) at that temperature (3). Phase solubility limits decrease at lower temperatures. At room temperature the solid solution is the matrix and minor amounts of a number of secondary phases are located at grain boundaries and within the grains. This faithfully represents the parent metal and most of the heat affected zone (HAZ).

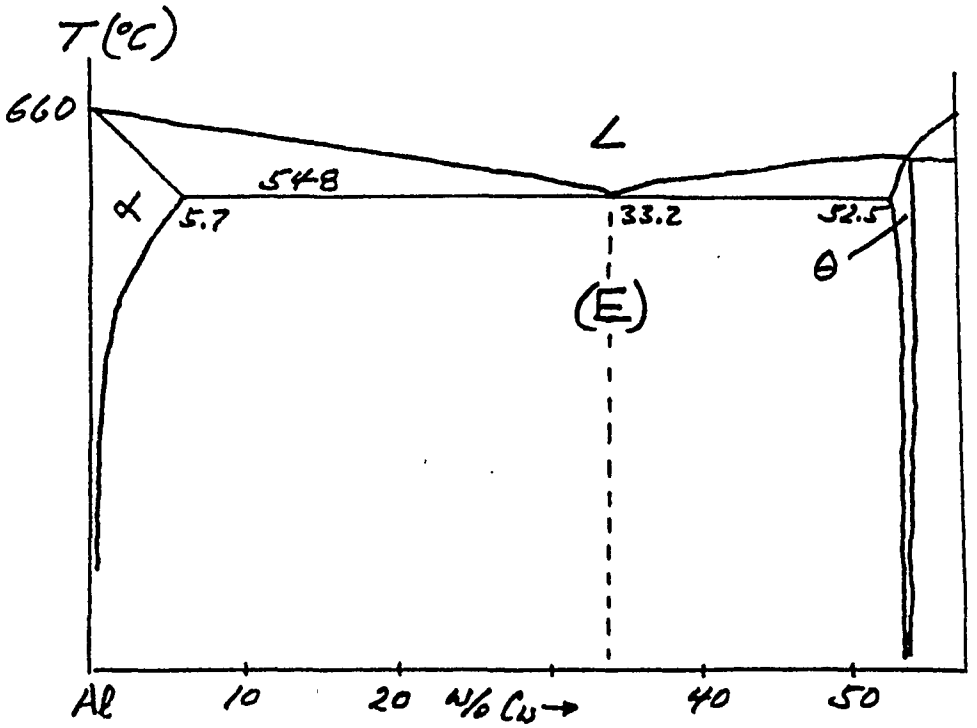

Figure 2. Aluminum rich portion of the Al-Cu binary equilibrium phase diagram. (10)

2. Structure.

Heat treatment to the T87 condition is a two step

procedure. The alloy is first solution annealed at 995 ^{o}F and then quenched in water to room temperature. In this condition the alloy is supersaturated with respect to copper. The elevated temperature soak saturates the solid solution with respect to the available alloying elements since solid solubility generally decreases monotonically with temperature and the quench is fast enough to cool the alloy before the copper precipitates out of solution as the intermetallic compound phase. Mechanically, the alloy is soft in this condition and has good ductility. However, it is unstable and tends to form the intermetallic compound at ambient temperature. 2024 aluminum alloy does this spontaneously at room temperature within about 48 hours. Alloy 2219 is designated T37 when it has been solution treated and cold worked 8%. It is designated T87 following a 24 hour aging treatment at 325 ^{o}F to achieve the desired condition (2). The changes that take place in the alloy during the ageing treatment are primarily the development of a finely divided, submicroscopic precipitate of the intermetallic compound phase. The increase in toughness of the alloy is attributed to the influence of the large number of submicroscopic hard intermetallic compound particles distributed throughout the grains of the alloy (4). The optimum particle is a 0.01 micron thick ellipsoidal platelet with a diameter of 0.03 microns. These particles interfere with the motions of dislocations. It is more difficult for the dislocations to glide, which raises alloy strength, but movement is still possible, thus retaining ductility. Further heating of the alloy, whether in the heat treating furnace or in the HAZ during welding, causes the submicroscopic particles to grow in size, decreasing in number and lose their strengthening effect.

3. Strength.

The mechanical characteristics of alloy 2219 are due to a number of contributing factors. Young's modulus and other elastic properties are constants for all metallurgical conditions. Strength is structure-sensitive and is controlled by chemistry, microstructure, and dislocation content. The grain size of a wrought alloy, such as 2219-T87 parent metal has a strong influence on strength. Yield strength is inversely proportional to the square root of the average grain diameter. This relation does not apply to the grains in the fusion zone, which have a different subgrain structure. The secondary dendritic branch spacing, which is a feature within fusion zone grains, is the applicable parameter (8). Hardness and yield strength are inversely proportional to the square root of this spacing.

Alloying elements are incorporated in two ways. Copper combines with aluminum to form the intermetallic compound, $CuAl_2$, which precipitates along grain boundaries and to a lesser degree within the grains. Other alloying elements in the formulation, especially manganese, form other second phase particles that can be seen in the microstructure. A portion of the 6.3% copper in the system is incorporated within the aluminum rich solid solution, which is the principal constituent of the microstructure. The chemical elements in solid solution modify strength and other structure-sensitive properties. The resulting solid solution strengthening is a component of the total alloy strength. The actual dissolved amount of any chemical species is a function of temperature and is, therefore subject to control through heat treatment.

Since yield strength is a measure of the stress required to move dislocations, any condition that impedes dislocation movement results in an increase in strength. Solid solution strengthening, decreases in grain size and secondary dendrite spacing, described above, have this effect. Any embedded particles, such as those large enough to be seen in the microstructure, also disrupt the continuity of slip planes and have this same effect. Second phase particles also have a stabilizing effect on the microstructure, in that they prevent grain growth (8,9). The submicroscopic, coherent particles that are produced by heat treatment in the age hardening process are much more effective in their dislocation blocking action. The development of this system of "hidden" particles throughtout each grain doubles the strength. The contributions to the strength of the age hardened alloy can be approximated in the following way:

a.	base strength (aluminum)	25%
b.	solid solution content	10%
c.	grain size control	10%
d.	dislocation content	10%
e.	age hardening	45%

The base strength represents the proportion of the total strength that is associated with typical, polycrystalline aluminum (with the addition of those second phase particles that are scattered throughout the grains). The other factors indicate their relative contribution to the strength of alloy 2219-T87.

The ultimate strength of the alloy either corresponds to the breaking strength or marks the onset of necking in a tensile test. Necking is a form of plastic instability

that occurs in tensile testing a ductile alloy. It is due to the production of vacancies and their accumulation into voids which counteract strain hardening. Vacancies and voids are produced within the metal during testing, and are not a part of the original microstructure (9). Since both plastic deformation and void production involve dislocation movement, there is a correlation between yield and ultimate strengths. The size of any hard particle (intermetallic compound or eutectic colony) in the microstructure plays a dominant role in the ultimate strength of the alloy because these particles act as vacancy and void sources. The larger the particles, the more effective void production, and the lower the ductility.

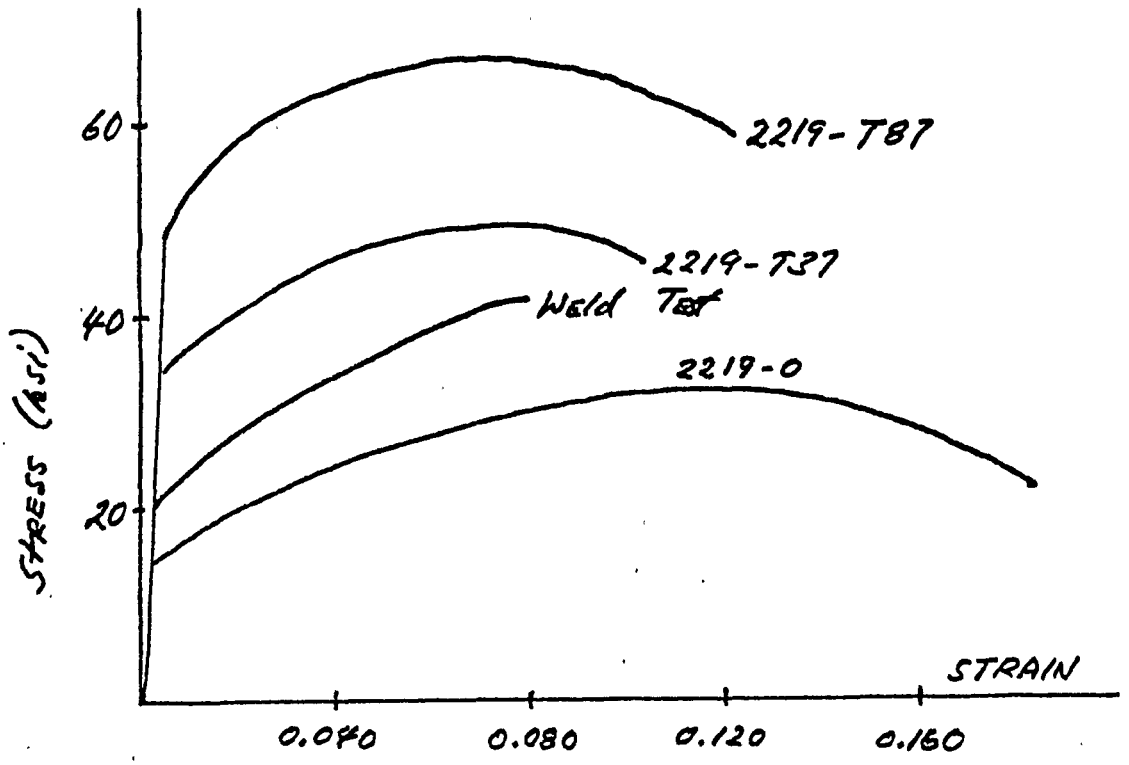

Figure 3. Stress strain curves for alloy 2219 in the fully annealed (2219-O), solution treated and 8% cold worked (2219-T37) and age hardened (2219-T87) conditions. The stress strain curve for a typical transverse weld test is included for comparison. (1,10)

The nominal values of yield and tensile strengths for the 2219-T87 engineering alloy are 56,000 psi and 67,000

psi, respectively. Various processing controls, based on the factors described above, can be used to either raise or lower these values. The upper limit in UTS attainable in aluminum base alloys appears to be 110,000 psi (alloy 7075-T6).

4. Weld Structure.

The fusion zone microstructure is produced by the eutectic transformation. The first solid to form on cooling is in the form of dendritic grains of solid solution, which was formed at temperatures above the eutectic. Since the solid solution composition is less than that of the average liquid in the weld puddle, the liquid is enriched by those alloying elements not frozen out. Enrichment occurs to a great enough degree that the eutectic constituent is formed between the dendritic branches. Based on the copper content of alloy 2219 the eutectic constituent is 2.2% by weight of the alloy.

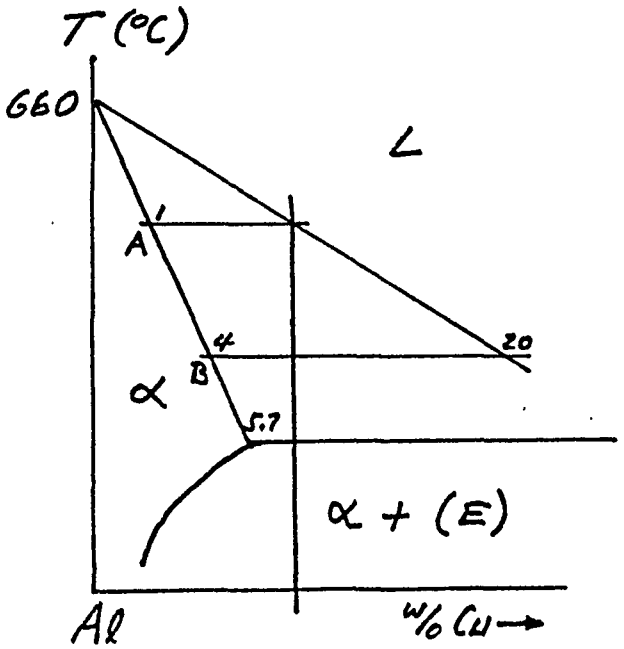

Figure 4. Phase diagram showing fusion zone compositions at start of solidification.

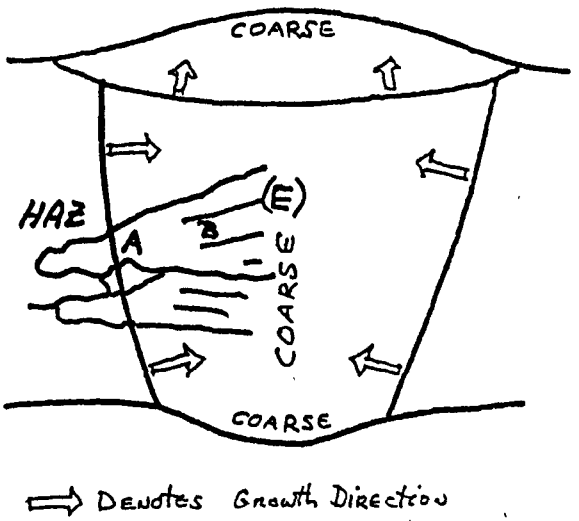

Figure 5. Fusion zone microstructure and growth direction.

The structure of the weld is best understood in reference to the aluminum-copper phase diagram. The composition of the liquid in the weld pool is based on the

average alloy composition (which will be used in this discussion), some dilution by filler metal and further modifications by segregation effects. The first solid to form is a dendritic solid solution of 1% Cu that forms at 623 C. Figure 4 is a portion of Figure 2 in which the average alloy composition and the composition of the first solid to form are shown. As solidification progresses the solidifying dendrites do not utilize all of the available copper, therefore the composition of the remaining liquid steadily increases. This is indicated by the lower isotherm marking equilibrium between a solid of 4% Cu and a liquid of 20% Cu. Chemical segregation effects actually cause the liquid composition to have a higher composition at the solidifying surface.

Finally the last liquid to freeze contains all of this excess copper. The copper-enriched solid is an eutectic mixture with an average composition of 33.2% copper, by weight. The eutectic is a lamellar mixture of solid solution and $CuAl_2$ intermetallic compound. Dendrites grow in alignment with the principal direction of heat transfer, which is into the adjacent parent metal. In the cover pass, which is not a keyhole weld, cooling is into the unmelted portion of the first weld pass. The sequence of structual transitions is similar in many respects to the transitions from the parent metal HAZ into the keyhole fusion zone.

There is a HAZ in both the parent metal and the preceding fusion zone in a multipass weld. Immediately adjacent to the fusion zone, where the alloy was melted totally, is a region where partial melting occurred due to normal chemical segregation within the original grains of the parent metal. Adjacent to this are zones where the alloy was subjected to various elevated temperatures for various periods of time. In alloy 2219, second phase particles are not dissolved to any appreciable extent below the eutectic melting temperature, therefore there is no pronounced region of grain growth. However, the typical microstructure indicates that the condition of the alloy has been changed, primarily with respect to overaging of the heat treated structure and modifications of the alloying element solution conditions.

Mechanical characteristics and properties are related to the chemical and structural condition of the alloy in the way described above. The individual contributions of chemical and structural factors to strength can be approximated in the following way:

a.	alloy composition	30%
b.	metallurgical condition	30%
c.	weld geometry	10%
d.	dendritic spacing	10%
e.	hard particle size	20%

The individual contributions are evaluated in relation to their effect on plastic extension in the tensile test as well as their strengthening effect. For example, an increase in hard particle size does not have a noticeable effect on yield strength or hardness, but increases the void production process, effectively reducing ductility. A ductility of 10% Elong is typical for the welded alloy. Beil and Hahn relate a variation of approximately 10% in UTS to weld geometry (11).

Changes in the microstructure affect properties in the HAZ but the dominant change is in the much lower levels of mechanical properties in the fusion zone. Strength tends towards the values of the fully annealed alloy (yield and tensile strengths of 11,000 and 25,000 psi, respectively and a ductility of 18% Elong). The cooling rate is usually adequate to provide a degree of supersaturation in the fusion zone so that a partial recovery of strength by spontaneous age hardening occurs. This accounts for the measured yield and tensile strength levels of 21,500 and 41,000 psi in weld test samples.

Beil and Hahn (11) have conducted a comprehensive study of the metallurgical condition of this welded system. They identify a number of factors contributing to loss of strength. They place special emphasis on the segregation and accumulation of copper and on the role of microporosity. Their presentation provides a great deal of information and many valuable insights.

5. Filler Metal.

Filler metal composition is chosen to retain properties, match appearance and prevent the formation of corrosion couples. Alloying elements are added through the filler wire to compensate for elements lost through evaporation and to strengthen and refine the microstructure. Poorman and Lovoy (6) studied the effect of different alloying elements on weld strength of 2219-T87. They selected filler metal wires to provide varying amounts of titanium and beryllium and to vary the copper:magnesium ratio. They found the results to be encouraging with respect to potential improvement of weld mechanical properties, but recognized that more testing is

required to make a change in production methods. The need now exists to perform a similar investigation with the VPPA process.

6. Summary

The effect of welding on properties is related to the redistribution of alloying elements in the fusion zone, the modification of microstructure in the HAZ, the production of a completely new microstructure in the fusion zone and a pattern of residual stresses. The dendritic spacing and the size of the interdendritic constituent are the most significant aspects of the new fusion zone microstructure. This constituent is produced under the slowest cooling conditions in both the keyhole and cover pass weld puddle. The size of this constituent is largest at the last part of the structure to freeze, where cooling is the slowest. Since cooling rate is the dominant factor affecting particle size, the intermetallic compound and eutectic particles are large. The differences in yield strength between the parent and weld metals are due, primarily, to metallurgical condition with respect to age hardening. Other factors are secondary. Tensile strength differences, however, are due to the differences in particle size. The largest particles in the wrought alloy microstructure are smaller, by at least an order of magnitude, than those in the weld fusion zone.

Theory of Mechanical Characteristics

The weld tensile sample is normally clamped in the tensile machine by flat, serrated wedge grips, compressing the sample ends (parent metal) in the welding direction. In this orientation, the least bending moment is applied to the sample during the test. The loading configuration involves the in-line separation of laterally constrained grips. Nunes analyzes this test configuration on the basis of a soft interlayer model (13). Bending moments are concentrated in the sample at the grip ends and at the edges of the crown and root reinforcement. Elastic stresses are soon driven to the yield at these points with the result of local cold work and other structural damage to the sample. Cold work where the base metal is gripped is of no serious consequence to test results, but concentrated, early deformation at the other points influences the magnitude of the test results as well as the features of the fracture surface. The magnitude and direction of peaking (angular distortion across the weld) influences the crack starting position.

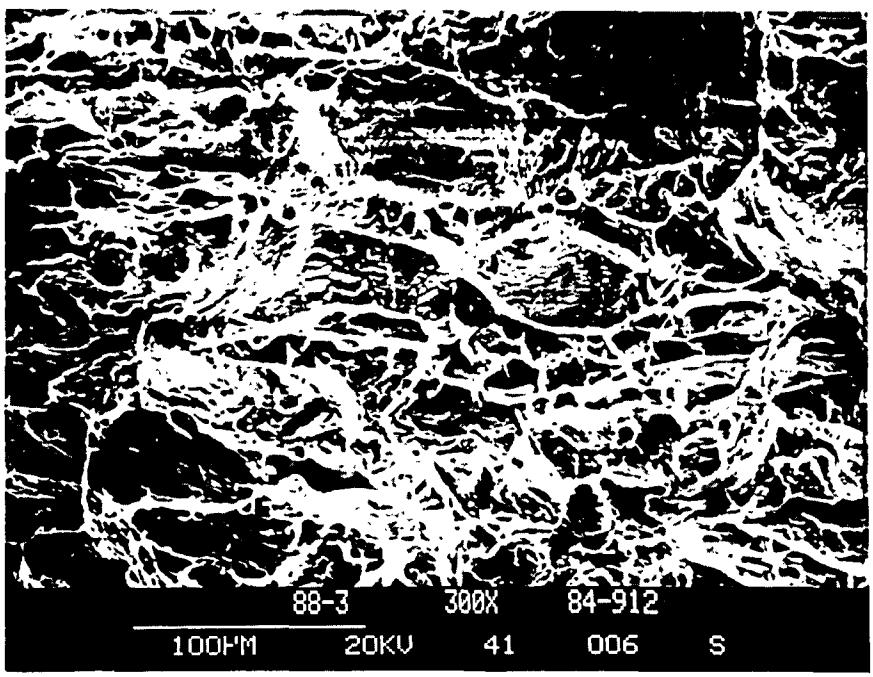

Figure 5. Normal dimple rupture. Average cell diameter, 23.3 microns; maximum cell diameter, 80.8 microns; and particle diameter, 55.6 microns.

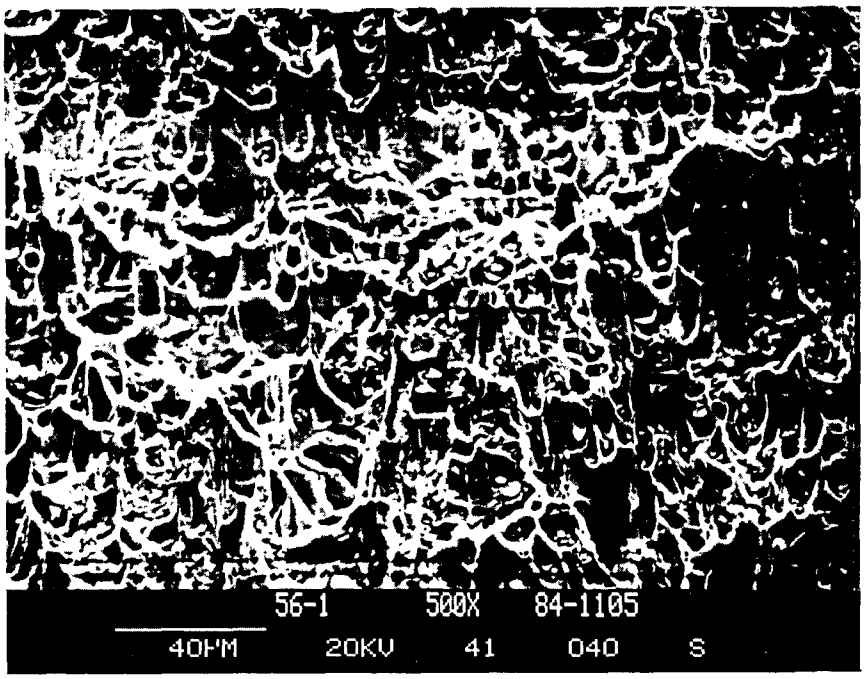

Figure 6. Shear mode dimple rupture.

For the usual case where only small amounts of sample compliance are required, the test continues through the typical stages of general plastic flow in the weld nugget and adjoining regions and finally into appropriate fracture processes. The dominant fracture process in welded 2219-T87/2319 is dimple rupture. Dimple rupture is illustrated in Figures 5 and 6. In Figure 5 dimple rupture occurred under conditions of tensile extension. The dimple rupture in Figure 6 occurred in shear. The dimples are open ended in one direction indicating that the sample was deforming in this manner as the dimples developed. In none of the welds has any other matrix fracture surface feature been observed.

Void production is a process that occurs in two stages at positions throughout each grain of the deformed metal. The first stage is the nucleation of stable voids of a critical size by the interaction of dislocations with hard, second phase particles, grain boundaries or slip bands. The second stage, which leads to dimple rupture, involves

the exaggerated stretching of matrix metal due to unimpeded dislocation glide out of the clean metal surface. This glide involves dislocation multiplication but no dislocation buildup and therefore continues until the metal is thinned to the point of total separation. The entire fracture surface is then covered by a network of cell walls, stretched by this process.

Each cell contains a point of nucleation and possibly a trace of the structural feature involved in void nucleation. Cell size directly depends on hard particle size. There is a characteristic second phase, or eutectic constituent particle size for each welding process depending on alloy system, welding power and speed, chemical segregation in the puddle and factors connected with the ambient and consumables.

The only evidence of brittle failure is within a few hard particles themselves. These particles are usually separated from the matrix, which is a dendritic solid solution. In a number of cases the particle appears to be directly exposed, but in most there is a small layer of solid solution over the surface. Since the void nucleation process involves interactions with dislocations, the process is more likely to occur with the larger particles that intercept a greater number of slip planes. Larger particles allow void production to become critical at lower levels of plastic deformation. Therefore, the tensile strength of the sample is reduced by large, hard particles. Conversely, tensile strength is improved by reducing the size of second phase particles.

Void production is not directly related to alloy yield strength, except in relation to dislocation movements. Yield strength is a measure of the initial motions of dislocations in the sample. The UTS depends on void production. Ductility is directly controlled by the dominant fracture process.

Experimental Procedures

The initial assignment to this research activity was by means of the following tasks:

1. determine the effect of the relation of rolling direction to welding direction,
2. determine the relation of parent metal to weldment strength,
3. compare the grain structures of samples welded at MSFC and MAF/MMC,
4. and determine the effect of impurities in the filler wire.

In considering these tasks and reviewing a number of test samples from an active weld qualification test program conducted by staff of both MSFC and MAF/MMC, a number of specific goals were identified to provide results for each of the tasks and to contribute to a coherent report on the structural weldability of aluminum alloy 2219-T87 by the VPPA process. These goals are listed and described in the following paragraphs.

Goal 1. (Tasks 1 and 2) A program of comparison welding of panels with rolling direction aligned in the welding direction and others aligned across the welding direction provide for the first two tasks. After assembly (tack welding), but before welding, test strips were cut transverse to the intended welding direction and machined into "dog bone" tensile test bars with 3/4 inch guage width. After welding each panel, weld test bars were cut, numbered and finish machined for tensile testing. These were machined to the standard 1 inch finished width. The samples provided enough information to compare the effect of weld/rolling direction alignment with base metal characteristics.

Goal 2. (Task 3) This activity was conducted by studying available samples from the recent 0.800 inch weld test qualification program. A total of 121 samples were available. Of these 78 had acceptable test results and 43 did not qualify as acceptable. It must be pointed out that all test results were within a narrow range. All welds had a good appearance and none contained any internal defects. Of the 78 acceptable samples, 54 were prepared with a J-groove configuration and 9 were shaved for testing.

Goal 3. (Task 4) The study of the effect of impurities in the filler wire was based, primarily, on

welding panels using M-934 filler wire. This filler alloy provides elements that modify the characteristics of the weld metal and was found to impart better mechanical properties over most of the temperature range of interest than other fillers as evaluated in TIG welding in a study reported on by Poorman and Lovoy (6).

Goal 4. Preliminary results of the examination of weld qualification test fracture surfaces indicated the presence of large particles in the region of fracture initiation. A program to control the maximum particle size in the weld, by controlling cooling rate, was planned to study this effect. Cooling rate in the weld was increased by the use of water cooled copper blocks which were attached to the plate surface along the upper half of the weld track. Plate thickness was 0.500 inches in this series of welds.

Goal 5. Understanding the exact conditions for the formation of the microstructure in the fusion zone is fundamental to the interpretation of test results and weld characteristics. A study was initiated to experimentally evaluate features of the microstructure by sectional metallographic examination, using quantitative procedures to every possible degree, and by direct examination of the solidifying surface in the keyhole.

Experimental procedures involved VPPA welding square butt joints of 2219-T87 aluminum alloy plates in the vertical up orientation. Filler wires were aluminum alloy 2319.

Standard static tensile test procedures were followed to determine yield strength, tensile strength and percent elongation. %Elong is calculated on the basis of a gauge length of 2 inches. Fracture surfaces were inspected visually for the source of fracture and for other details of the fracture surface. Scanning electron microscopy (SEM) was used to identify and measure fracture surface features. The measurements were made on photographs. The energy dispersive x-ray analysis attachment to the SEM was used for microchemical analysis to confirm the identity of features. Metallographic analyses were performed using standard methods and Keller's etch.

Results and Discussion

1. Goals Results.

Goal 1. Four samples of parent metal were cut from each weld test panel parallel to the weld test samples. Therefore, there are 12 tests of the parent metal in the rolling direction and twelve tests across the rolling direction. Test results are summarized in Table 1. Each line lists the average values of test results from four test bars of the indicated panel. The average and standard deviation are calculated for the 12 samples from the three average values listed immediately above.

Table 2
Parent Metal Mechanical Properties

Panel Number	Y.S. (psi)	U.T.S. (psi)	%ELONG (%)	ORIENTATION
1072	54,914	67,077	16.7	Cross
1079	54,896	67,171	16.3	"
1080	56,859	69,027	15.2	"
Ave.	55,556	67,758	16.1	"
S. Dev.	1,128	1,010	0.78	
1081	56,272	68,957	13.6	Parallel
1082	55,186	68,161	14.5	"
1083	55,985	69,007	13.1	"
Ave.	55,814	68,708	13.7	"
S. Dev.	563	475	0.71	

These results show a small difference between ultimate tensile strength measured with the rolling direction and across the rolling direction. As expected, tensile loading parallel to the rolling direction yields the higher strength and lower ductility. This difference is due to the difference in effective grain boundary spacing available for slip. The measured increase of UTS above the reference yield is 7.4%, which is accounted for by a grain shape aspect ratio of 1.33, which corresponds with measurements.

Weld test results are listed in the following table.

Table 3
Weld Test Results

Panel Number	Y.S. (psi)	U.T.S. (psi)	%ELONG (%)	Orientation
1072	21,685	38,695	7.4	Parallel
1079	20,012	37,882	8.0	"
1080	20,444	36,371	6.5	"
Ave.	20,714	37,649	7.3	"
S. Dev.	868	1,179	0.75	
1081	20,748	36,609	6.6	Cross
1082	19,057	37,846	7.4	"
1083	20,749	35,754	6.6	"
Ave.	20,185	36,736	6.9	"
S. Dev.	977	1,051	0.46	
1094	19,099	37,072	6.4	Parallel
1095	19,250	37,987	7.1	"
1096	18,889	39,282	8.5	"
Ave.	19,079	38,114	7.3	"
S. Dev.	181	1,110	1.07	
1098	18,715	36,509	5.9	Cross
1099	18,939	37,375	6.9	"
1100	19,103	36,404	6.6	"
Ave.	18,919	36,763	6.5	"
S. Dev.	195	533	0.51	

These results show that the mechanical properties are better if the weld is made parallel to the parent metal rolling direction. This corresponds to current practice. It is unfortunate that the weld test results do not meet specifications of 38 ksi average UTS and minimum sample test of 35 ksi, excepting one set. Never-the-less, for purposes of comparison these test results favor the present practice with respect to orientation of weld direction.

Fracture surface examination shows the same pattern of fracture surfaces reported on under the Goal 2 results.

Parent metal test bar fracture surfaces have a cup and cone profile. Fracture initiated at the center of each sample in a dimple rupture mode and progressed onto shear separation faces, oriented approximately 45 degrees to the loading direction. The fracture mode on these shear faces is also dimple rupture.

Goal 2. A detailed examination of the fracture surfaces of the 121, 0.800 inches thick weld qualification test samples revealed a number of fracture paths. However, it is clear that in all cases, fracture initiated within the fusion zone. The point or region of crack initiation was indicated by several features, which include:

1. A series of fracture path ridges emanating from the fracture source.

2. The longest transverse fracture surface edge, indicating separation with the least plastic deformation (plastic deformation and lateral contraction increase steadily with crosshead movement until separation occurs, thus the amount of deformation provides a record of test time).

3. The position between the two fracture surfaces with the greatest residual separation (this feature also indicates relative time of separation by the principle of progressive permanent deformation).

SEM examination of the fracture surfaces revealed that all surfaces were of the dimple rupture type. Large eutectic or intermetallic compound particles were retained, embedded within dimples on the fracture surface in the region of crack initiation. Most of the larger particles appear to have been fractured and a smaller number appear to have simply been separated from the matrix close to the interphase boundary. Figure 7 shows several eutectic particles. Several cracks are visible. Hartbower et. al. (16) and Heiple and Carpenter (17) report on the cracking of particles during tensile testing, using acoustic-emission techniques. Butcher and Allen (15) have modeled the conditions that lead to fracture or separation of a hard particle in a ductile matrix. Microchemical analysis (Figure 8) in the SEM using the EDAX attachment clearly shows that these large particles contain more copper than the general alloy.

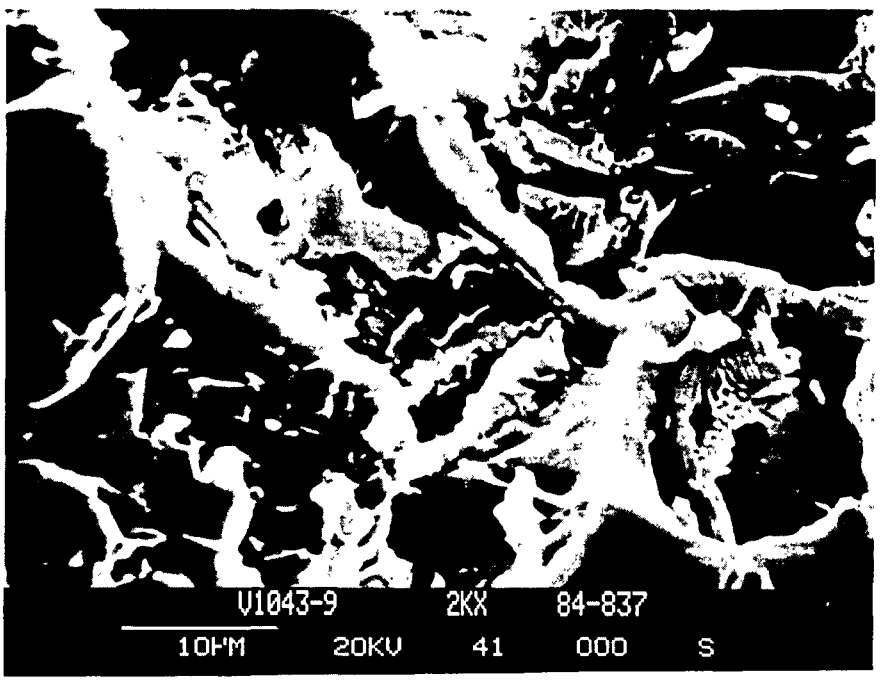

Figure 7. Dimple rupture fracture surface with large eutectic colony particle retained in the large dimple.

SEM analysis was conducted on one sample from each of the groups available. It was not possible to conduct a thorough analysis of each sample. One of the two fracture surfaces was cut from the remaining test bar and bonded to a specimen stage with graphite lacquer, which is electrically conductive. The initial examination procedure involved scanning the entire fracture surface, searching for the region containing the largest particles. Photographs were taken at several candidate locations for later comparison and measurement. The procedure was soon modified by outlining the fracture start region on the

fracture surface, with a soft pencil. The region of crack initiation was identified as described above. This procedure reduced the time required for the analysis and provides a record of the region. A photograph was then made of the spot that contains the largest particle within the marked region.

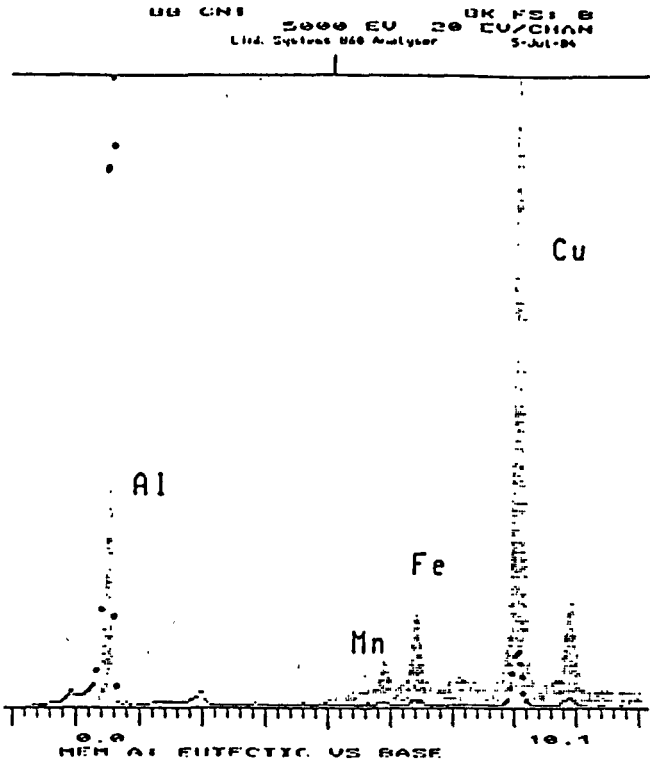

Figure 8. Microchemical analysis of a large particle (a) and the general background of the sample (b).

All subsequent measurements were made from the prints. These measurements included the length of the magnification calibration bar, a count of dimple wall intersections on a randomly placed test line, largest transverse rupture cell diameter and largest transverse interdendritic particle diameter. Processing this data led to measurements of the average cell diameter and maximum cell and particle diameters, in microns. Of the 22 samples evaluated, the test results from two were discarded as being anomalous. The measured particle sizes were out of the range of values for the other samples. Figure 9 is a plot of UTS

versus maximum particle size and figure 10 displays plots of UTS versus the average cell and particle diameters.

The lines drawn through the data points are computed lines. In Figure 9 the line represents all twenty data points shown. In Figure 10, the line represents only the

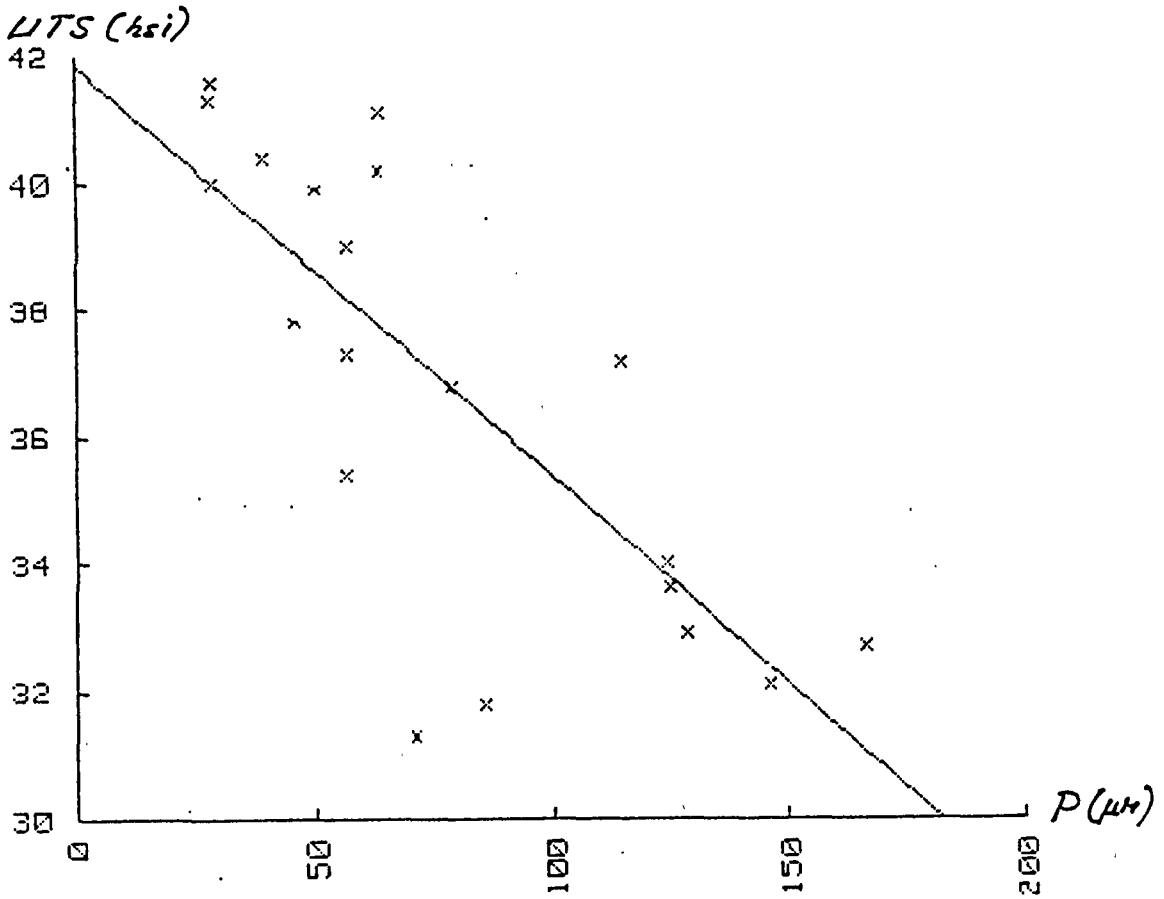

Figure 9. UTS versus largest interdendritic particle size for 0.800 inch VPPA weld test bars of 2219-T87 aluminum plate welded with 2319 filler wire.

20 largest size values. These are the maximum cell diameter values. The other 20 points are the average cell diameters.

Figure 10 indicates the possibility of a trend between tensile strength and largest rupture cell diameter, but the scatter overshadows any such trend. There is no apparent trend between UTS and average cell size. The average,

background dimple rupture cell is related to the average, interdendritic particle size, which is closely related to the secondary dendritic branch spacing.

Goal 3. The effect of impurities on VPPA welding is similar to impurity effects on the TIG process. The investigation of this effect was limited to one demonstration involving the intentional contamination of the weld metal with traces of oil prior to welding. The resulting weld showed an irregularity of form that is very

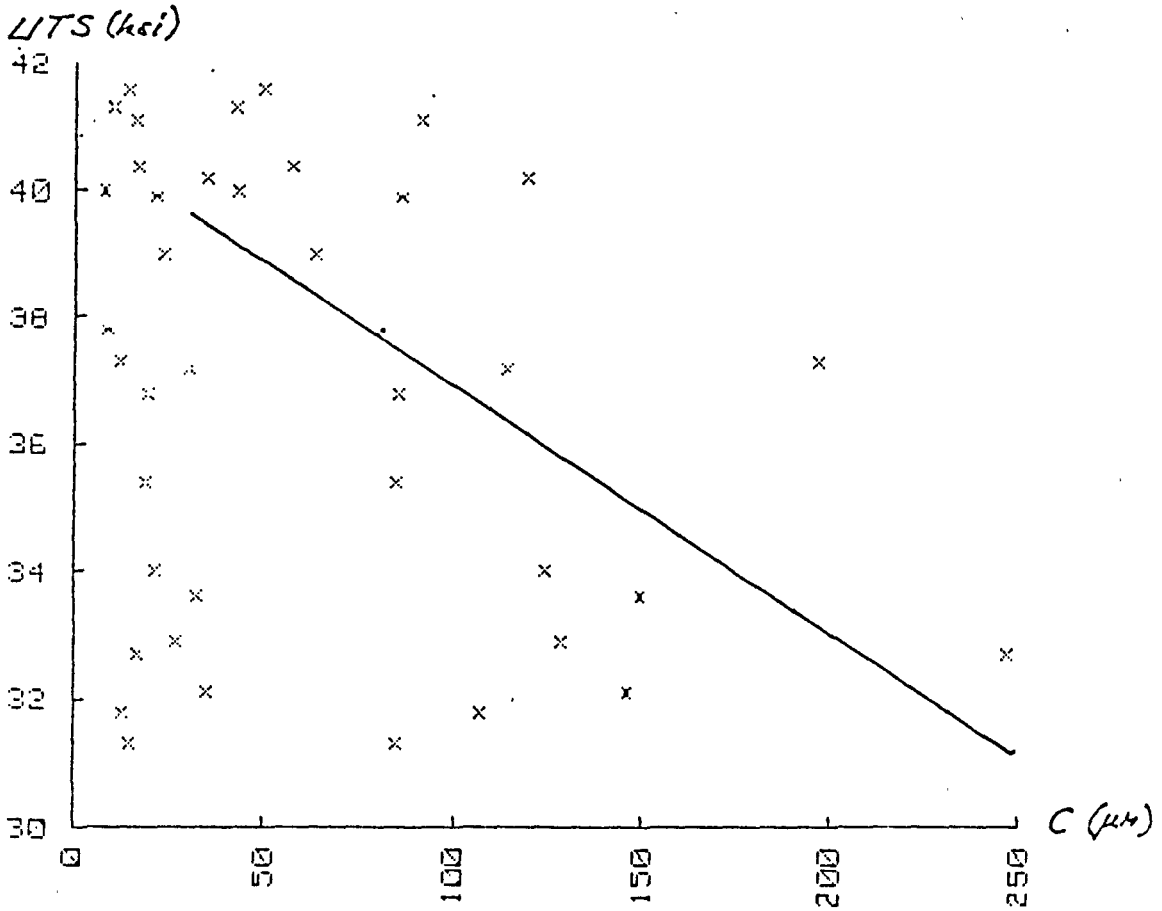

Figure 10. UTS versus largest and average dimple rupture cell diameter on samples represented in Figure 9.

similar to that reported in TIG welding and attributed to the surface activity of the contaminant. This strongly suggests that the keyhole liquid supports currents that are subject to such factors. Additionally, the resulting weld metal included a series of fusion boundary cracks and

porosity in the fusion zone.

The effect of alloy M-934 filler wire on weld test results is shown in the following table, which includes comparable test results reported on in the Goal 1 report. The values listed for 2319 filler metal are copied from Table 3. In both cases, welding was parallel to the rolling direction. The test results compare two groups of 19 samples welded with M-934 filler with two groups of 36 samples welded with the standard 2319 filler wire.

Table 4
Filler Wire Weld Test Comparison

Filler Metal	Y.S. (psi)	U.T.S. (psi)	%ELONG (%)
M-934-1	22,655	37,446	5.8
S. Dev.	591	996	0.38
2319	20,714	37,649	7.3
S. Dev.	868	1,179	0.75
M-934-2	22,014	39,406	6.0
S. Dev.	400	1,631	0.73
2319	19,079	38,114	7.3
S. Dev.	181	1,110	1.07

The results show a higher yield strength countered by a lower ductility. The UTS is slightly lower, but not significantly. This filler alloy does not appear to improve the microstructure. The difference in yield strength is attributed to the solid solution strengthening effects due to the differences in alloy composition. The increase in UTS in the second group welded with M-934 filler wire is not considered to be significant.

Goal 4. The mechanical test results for four panels are listed below. In this table, the welds made in the cooled region are presented first. On the data sheets the samples are designated 1a, 2a, 3a and 4a. The samples that were welded away from the cooling blocks, numbered 5b, 6b,

7b and 8b on the data sheets, are listed as the last four groups.

Cooling produces a significant increase in both yield and tensile strengths at the same level of ductility. In panels 1087 and 1088 the cover pass did not adequately cover the fusion zone of the root pass, but the relationship of the two passes was proper in panels 1089 and 1090. A second distinction is that the cooling blocks were set closer to the weld center line in the second two panels and a 5 ampere adjustment in the plasma current was

Table 5
Cooling Effect Weld Test Results

Panel number	Y.S. (psi)	U.T.S. (psi)	%ELONG (%)	Condition
1087	22,110	39,971	5.5	Cooled
S. Dev.	151	264	0.0	
1088	21,876	41,008	5.9	"
S. Dev.	235	613	0.25	
1089	21,877	41,024	6.0	"
S. Dev.	344	343	0.0	
1090	24,607	39,621	5.6	"
S. Dev.	465	1,376	0.48	
Ave.	22,617	40,406	5.8	"
S. Dev.	1,331	719	0.24	
1087	21,304	38,754	5.5	Uncooled
S. Dev.	449	512	0.0	
1088	21,495	40,179	6.0	"
S. Dev.	235	277	0.0	
1089	21,251	38,777	5.8	"
S. Dev.	457	595	0.29	
1090	20,636	39,283	5.5	"
S. Dev.	190	445	0.0	
Ave.	21,172	39,248	5.7	"
S. Dev.	372	667	0.24	

made when the weld passed into this region in panel 1089 only. The cooling block spacings were 3.0 and 2.0 inches across the weld in the first two and second two panels, respectively.

Goal 5. The temperature and pressure of the plasma liquify an ellipsoidal plug of alloy through the plate. The conical profile of this plug is revealed by the final shape of the weld in cross section. The dominant components of fluid flow are downwards by gravity and forward under plasma pressure. This flow of liquid naturally forms a reinforcement at the root and a groove at the torch side, if not built up by filler metal additions. Excessive plasma pressure results in cutting.

Solidification begins at the widest part of the cone as the source of heat moves on. This solidification is in equilibrium with alloy of almost average composition and at a very low growth rate within the boundary layer of liquid. The liquid, immediately adjacent to the solid is

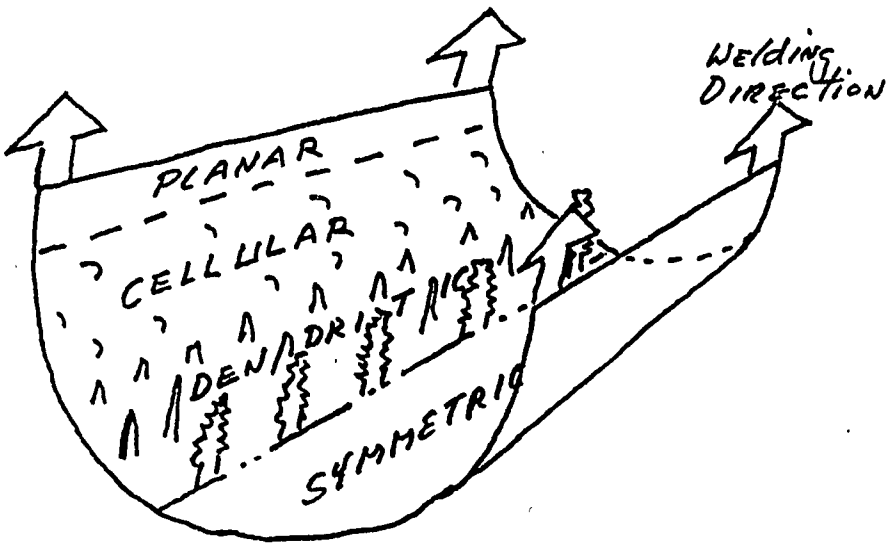

Figure 11. Map of the keyhole solidification surface (schematic).

essentially static due to frictional effects. The new solid is typically a product of epitaxial, planar growth. Grain structures of the HAZ are continued into the fusion

zone. Since the liquid originates, primarily, out of the plate itself., with only a small fraction remixed, and solidifies as it flows, the first portion to solidify is dilute, thus enriching the liquid that flows on.

While liquid freezes at the sides, as described above, solidification also occurs at all surface positions further back around the keyhole. The weld metal composition varies continuously, and is enriched by most alloying elements. Figure 11 is a perspective representation of the surface on which solidification occurs. Alloy composition varies continuously from the line of start to the line of finish. The actual temperature also varies. The surface structure also changes from smooth (planar growth), to cellular (with slight projections) to cellular dendritic (extended projections) and to branched dendritic. At all positions, solidification occurs within the boundary layer that is effectively not moving, so that chemical equilibrium is approximated. The composition of the planar surface is less than that of the branched dendritic surface. Equilibrium is local so that enrichment extends beyond that expected in ingot solidification.

2. Discussion.

The strength of a welded panel depends on a number of coupled factors. The composition of the base metal and modifications by the filler metal govern the dimensions of structural features in the weld metal. Both composition and structural size (as represented by secondary dendrite branch spacing) directly affect alloy strength. For a given composition, spacing is controlled by cooling rate, which is in turn governed by energy input into the weld and other welding parameters and any preheat. The application of the cooling blocks illustrated this effect since there was an increase in strength and toughness.

A variety of factors were considered and studied. The controlled study of alignment between the welding direction and rolling direction of the plates showed that the present practice, is the better of the two. This result is contrary to the effect of rolling direction on base metal strength. In that case, the greater number of grains in the sample cross section increases both the yield and tensile strengths. In the welded sample, the HAZ grains do not reflect the differences in grain dimension with orientation, probably due to recrystallization effects, so that this size effect does not affect fusion metal microstructure and properties in the same way. The pattern

and direction of residual stresses from the base metal cold work also participate in these relations.

The development of the microstructure of the weld metal is a governing factor. This process involves a number of factors within the liquid in the keyhole. Nunes describes the weld pool (not keyhole) using a mathematical model and describes circulation (14). Plasma temperature, dimensions and pressure are important, but the formation of the final microstructure takes place under the liquid in the keyhole, away from direct contact with the plasma. Growth of the metal begins at the side of the keyhole and continues to develop at different positions, finally along the center line. In vertical up VPPA welding the final microstructure reveals this pattern of growth and shows that liquid flow contains a dominant downward component on each side of the keyhole. One might anticipate a vortex component, but there is little or no evidence for it. There is probably an axial (relative to the keyhole) component forced by momentum transferred from the plasma. This axial component may produce a pattern of circulation, but no direct evidence has been found.

The test procedure is important to the measurement of properties. For valid comparisons, test bars must have the same nominal dimensions. They must also be gripped in the same manner, with the same constraints. The reason for both requirements is the dependence on the moment distribution and stress field in the test bar. The orientation of these fields in the vicinity of the reinforcement is critical. Test performance depends on the interaction of the applied stress field with the shape/property field of the weld test sample. During the progress of testing, different portions of the sample respond differently to the stresses, but each part of the sample responds in the sequence of elastic deformation; joined by plastic deformation; joined by void production and accumulation; resulting in separation. Separation begins in that part of the sample that was the first to pass through the deformation stages.

There is an elastic response to each component of the stress field. In a face centered cubic alloy, such as 2219-T87, there are many available slip systems within each grain to support plastic deformation. Plastic deformation, which occurs only in response to shear stress components, favors action on planes inclined to the tensile direction. However, the dimple rupture process, is in response to longitudinal tensile stress components. Dimple rupture is the common fracture process that produces the starting

crack in a typical "cup and cone" tensile test. This crack starter responds to the initial longitudinal stress in the test bar. The effect of the lateral constraint and triaxial stress state is relatively minor. Once the center crack has formed, the stress state changes from one of dominant longitudinal tension to a shear stress condition. The shear surfaces on the side walls of the cup and cone are also dimple rupture surfaces. However, the dimples are open ended, pointing in the shear direction. This description applies to tensile test specimens from many alloy systems including 2219-T87. Most of the fracture surfaces of the weld test specimens that have been studied in this research are cup and cone fractures. The others are also of the dimple rupture mode. In every case fracture began in the fusion zone and progressed through the fusion zone. The differences observed between the shapes reflect variations on the above pattern. In one extreme variation, the fracture surface extends completely through the weld on a near 45 degree diagonal surface. In this case, even the crack starting region, which involved void formation under the action of longitudinal stresses, is on an inclined, stepped surface, in approximate alignment with the shear surfaces. Dimple rupture is the only mechanism over the entire surface.

It was found that the interdendritic particle size correlated with UTS in one series of samples. A variation of 150 microns in particle size correlates with a 10 ksi variation in UTS. In a second series, the variation of UTS was so restricted the correlation was not clearly displayed. However, there is general agreement among metallurgists that particle size is the dominant variable in the void production process. This applies equally to particle crack nucleation as well as to nucleation by dislocation interactions. Particle cracking appears to be the important process for crack nucleation in welded 2219-T87 aluminum plate.

3. Conclusions

It was very apparent that this welded system is ductile, in that all fracture surfaces were totally of the dimple rupture mode. Fracture initiated in the fusion zone and generally followed a pattern of "cup and cone" separation. In a small fraction of the samples, fracture crossed the weld on a relatively planar surface.

The UTS correlates with the largest dimple rupture cell size and the largest interdendritic particle size. The range of variation is approximately 20% of the UTS.

Specifically, a variation of 150 microns particle size was found to correlate with 10 ksi UTS.

It was found that base metal cooling increases both strength and toughness.

Welding parallel to the rolling direction, which is the current practice, is recommended.

Bibliography

1. John Sessler and Volker Weiss, Materials Data Handbook, Aluminum Alloy 2219, Department of Chemical Engineering and Metallurgy, Syracuse University, Contract NAS8-11345, (1966), NASA/MSFC, Sponsor.

2. Ray M. Hart, Alcoa Green Letter: Alcoa Aluminum Alloys 2219 and 2419, Aluminum Company of America, (1983).

3. L. F. Mondolfo, "Aluminum-Copper System," Aluminum Alloys, Structure and Properties, (1976), 253-278.

4. H. K. Hardy, "The Ageing Characteristics of Some Ternary Aluminium-Copper-Magnesium Alloys with Copper:Magnesium Weight Ratios of 7:1 and 2.2:1," J. Inst. Metals, 83, (1954-55), 17-34.

5. C. R. Heiple and S. H. Carpenter, "Changes in Acoustic-Emission Peaks in Precipitation Strengthened Alloys with Heat Treatment," J. Acoustic Sciences, 1, No. 4, (1983), 251-262.

6. R. M. Poorman and C. V. Lovoy, "Improved TIG Weld Joint Strength in Aluminum Alloy 2219-T87 by Filler Metal Substitution," NASA Technical Memorandum NASA TM X-64659, (1972).

7. Personal communication, W. A. Wilson, MSFC.

8. M. C. Flemings, Solidification Processing, (1974), McGraw-Hill, p. 146 ff.

9. K. Easterling, Introduction to the Physical Metallurgy of Welding, (1983), Butterworths, p. 70 ff.

10. "Aluminum Alloy 2219, Plate and Sheet," Federal Specification Sheet, QQ-A-250/30A, (November 19, 1982).

11. R. J. Beil and G. T. Hahn, "The Influence of Weld Process Variables on Crack Initiation and Growth In 2219-T87 Aluminum TIG and VPPA Weldments," Final Report to Martin Marietta Corporation, Contract No. AS 3-756222, (30 September 1983).

12. A. C. Nunes, Jr., E. O. Bayless, Jr., C. S. Jones III, P. M. Munafo, A. P. Biddle, and W. A. Wilson, "The Variable Polarity Plasma Arc Welding Process: Its Application To The Space Shuttle External Tank," to be published.

13. A. C. Nunes, Jr., H. L. Novak, and M. C. McIlwain, "Weld Geometry Strength Effect In 2219-T87 Aluminum," NASA Technical Memorandum NASA TM-82404, (March 1981).

14. A. C. Nunes, Jr., "An Extended Rosenthal Weld Model," Welding Journal, 62, (June, 1963), 165-s - 170-s.

15. B. R. Butcher and P. L. Allen, "Tensile Flow and Fracture at Large Inclusions," Metals Science, (October, 1977), 462-469.

16. C. E. Hartbower, W. G. Reuter, C. F. Morris and P. P. Crimmins, "Correlation of Stress-Wave-Emission Characteristics With Fracture in Aluminum Alloys," NASA Contractor Report NASA CR-2072, (July, 1972).

17. C. R. Heiple and S. H. Carpenter, "Changes in Acoustic-Emission Peaks in Precipitation Strengthened Alloys With Heat Treatment," Journal of Acoustic Science, 1, (October, 1982), 251-262.